Focussed on the Failure Analysis of Materials and Structures

Visual Abstract

# Predictive modelling of creep crack initiation and growth using Extended Finite Element Method (XFEM)

Meor Iqram Meor Ahmad, Mohd Anas Mohd Sabri, Mohd Faizal Mat Tahir
*Department of Mechanical and Manufacturing Engineering, Faculty of Engineering and Built Environment, Universiti Kebangsaan Malaysia, 43600 UKM Bangi, Selangor, Malaysia*
*meoriqram@ukm.edu.my, anasms@ukm.edu.my, mfaizalmt@ukm.edu.my*

Nur Azam Abdullah
*Structural Mechanics and Dynamics Research Group, Department of Mechanical Engineering, International Islamic University Malaysia, Kuala Lumpur, Malaysia*
*azam@iium.edu.my*

**ABSTRACT.** In this study, a numerical strategy for predictive modelling of creep in tension tests for the rectangular plate with a single crack and CT-specimen based on the extended finite element method (XFEM) will be described in detail. A model of creep fracture initiation and creep crack growth (CCG) is developed, while the XFEM is employed to spots located inside the finite element for the purpose of predicting crack potential and propagation. In order to characterize the creep fracture initiation, identification of C(t)-integral formula is conducted. In addition, XFEM and analytical solutions are also analyzed to look at the connection of C(t)-integral with time for a rectangular plate with a single crack under plane stress conditions. An illustration showing the sequence of stress distribution and displacement contour plots are also being presented. The stresses and displacements spread throughout the crack path have also been determined using CT-specimens. In addition, the creep cracks growth length with normalized time and the creep crack growth rate with the C(t)-integral are predicted to be related, indicating that the numerical results are in good accord with the experimental results.

**KEYWORDS.** XFEM; creep crack initiation and growth; C(t)-integral.

OPEN ACCESS

**Citation:** Meor Ahmad, M. I., Mohd Sabri, M. A., Mat Tahir, M. F., Abdullah, N. A., Predictive modelling of creep crack initiation and growth using Extended Finite Element Method (XFEM), Frattura ed Integrità Strutturale, 61 (2022) 119-129.

**Received:** 17.02.2022
**Accepted:** 18.04.2022
**Online first:** 27.04.2022
**Published:** 01.07.2022



## INTRODUCTION

It is a common practice in the industry in which elastic-nonlinear viscous materials must withstand long duration under cyclic loads at high temperatures as that of turbine blades in jet engines. The focus should be on creep when evaluating the materials' resistance to deformation and failure over lengthy period of time at extreme temperatures under specified loads. Creep is a plastic deformation process which is influenced by time and one of the main degradation mechanisms for

metals undergoing consistent stresses and temperatures ranging at approximately 0.3-0.5 of the melting point. Nucleation, growth and coalescence of cavities on the grain boundaries are the main causes of creep failure [1].
A predictive approach is needed to make sure a safe running of the component operation for a specified period of time. By employing a finite element technique, a substantial amount of attempts was conducted to estimate the deformation and assess the durability of creep failure. In order to predict the creep crack growth, Hsu and Zhai [2] have suggested a finite element algorithm that may provide detail stress and strain distributions, the kinematics of the inelastic areas and the growing crack profile.
The creep crack growth rates in the 32%-Ni-20%-Cr alloy Incoloy 800 H at 800°C was associated with the fracture mechanics parameter C* integral by experimental and numerical investigations as mentioned by Hollstein and Kienzler [3]. Yatomi et al. [4] then built a creep crack growth model to forecast the accelerated cracking at low C* values to deter-mine the trends between CCG rates at high and low C* values. It had been estimated and shown by Zhang et al. [5] that the creep crack growth behaviour in Cr-Mo-V steel specimen and interaction between crack tip stress states and stress-dependent creep ductility had resulted in the rise of a broad range of C*-integral.
The refinement of mesh to geometric discontinuities is required when predicting the stationary discontinuities using the conventional finite element method (FEM). It is necessary to capture enough singular asymptotic field in the crack tip area by means of mesh refinement. But modelling a growing crack is significantly more laborious because the mesh needs to be continually updated to reflect the geometry of the discontinuity when the crack advances. In 1999, the ex-tended finite element (XFEM) approach of Belytschko and Black was devised to relieve the weaknesses related to the meshing of crack surfaces. This strategy makes it easier to add local enrichment functions into a finite element approximation [6,7].
Special enriched functions in combination with additional degrees of freedom ensure the occurrence of discontinuities. Furthermore, earlier researches on XFEM have demonstrated that the method can alleviate computational challenges, particularly when it comes to crack growth analysis. The strain accumulation criterion was used to analyze fatigue crack growth in a three-point bending specimen using XFEM, and the simulation and experimental data were in good accordance [8]. Furthermore, there was a strong connection between the numerical and experimental data obtained when XFEM was used as a predictive tool to solve the problem of elastic fracture in the crack propagation of a chopped glass-reinforced composite during biaxial testing [9]. The XFEM was used to simulate creep crack growth in CT and CTS for P91 steel and 316 stainless steel at high temperature in the previous application [10]. Besides that, the XFEM was also carried out to model crack and crack growth behaviour in the power-law of creep materials [11].

## MATHEMATICAL FORMULATION

The constitutive law explains the elastic-nonlinear-viscous behaviour for uniaxial tension under small-scale creep conditions as:

$$\dot{\varepsilon} = \frac{\dot{\sigma}}{E} + B\sigma^{n} \tag{1}$$

where $\dot{\varepsilon}$ is the elastic strain rate, E is the Young's Modulus, B is the creep coefficient and $n$ is the creep exponent. The parameter C(t) describes the intensity of the near-tip fields in elastic-nonlinear viscous materials. The amplitude factor C(t), which is unknown from the asymptotic analysis, is influenced by elapsed time, remote load magnitude, crack configuration, and material properties. A self-similarity analysis conducted by Riedel and Rice [12] yielded the following relationship between J-integral and C(t) for planar stress:

$$C(t) = \frac{J}{(n+1)t} = \frac{K_I^2}{(n+1)Et} \tag{2}$$

Under steady-state conditions at long times, C(t)→C*. Ehler and Riedel [13] proposed the following approximate formula for C(t) between small-scale creep and extensive creep:

$$C(t) = C^{*}\left(\frac{t_T}{t} + 1\right) \tag{3}$$

where,

$$C^* = Bc\left(\frac{a}{W}\right)h_1\left(\frac{a}{W},n\right)\left(\frac{P\sigma_0}{P_0}\right)^{n+1} \tag{4}$$

$$t_T = \frac{K_I^2}{(n+1)EC^*} \tag{5}$$

where a is the crack length, W is the specimen width, c=W - a is the length of the uncracked ligament, $h_1$ is a dimensionless function of n, $\sigma_0$ is the reference stress, P is the applied stress, $P_0$ is an appropriate reference load, $K_I$ is the stress intensity factor and $t_T$ is the characteristic time for transition from small-scale creep to extensive creep introduced by Riedel and Rice [12]. For this study, however, the value of C(t) is determined by using the line integral as the following:

$$C(t) = \int_\Gamma W^* dy + \sigma_{ij} n_j \frac{\partial \dot{u}_i}{\partial x} ds \tag{6}$$

where,

$$W^* = \int_0^{\dot{\varepsilon}_{ij}^c} \frac{n}{n+1}\sigma_{ij} d\dot{\varepsilon}_{ij}^c \tag{7}$$

in which Γ is a vanishingly small counter-clockwise contour around the crack tip, n is the creep parameter, $n_j$ is the unit outward normal to Γ and ds is the arc length along Γ. $\partial \dot{u}_i$ is the component of displacement rate, W* is the strain energy rate density for the power law creep model, $\sigma_{ij}$ is the component of equivalent stress and $\dot{\varepsilon}_{ij}^c$ is the component of creep strain rate.

XFEM introduces a numerical model of crack initiation and propagation in which the approximation for a displacement vector function, $\boldsymbol{u}$, with the partition of unity enrichment is [14]:

$$\boldsymbol{u} = \sum_{i=1}^{n} N_i(x)u_i + \sum_{j=1}^{m} N_j(x)H(\xi)a_j + \sum_{k=1}^{mt_1} N_k(x)\sum_{\alpha=1}^{mf} F_\alpha^1(x)b_k^{\alpha_1} + \sum_{k=1}^{mt_2} N_k(x)\sum_{\alpha=1}^{mf} F_\alpha^2(x)b_k^{\alpha_2} \tag{8}$$

where $N_i(x)$ is the nodal shape function, $N_j(x)$ and are the new set of shape function associated with the enrichment part of the approximation. $u_i$ is the nodal displacement vector associated with the continuous part of the finite element solution, $H(\xi)$ represents a discontinuous jump function across the crack surfaces, $a_j, b_k^{\alpha_1}$ and $b_k^{\alpha_2}$ are the enriched nodal degree of freedom vector for modelling crack faces and two crack tips, respectively. $n$ is the number of nodes for each finite element, and $m$ is the set of nodes that have the crack face (but excludes the crack tip) in their support domain. While, $mt_1$ and $mt_2$ are the sets of nodes associated with crack tips 1 and 2 in their influence domain and $F_\alpha^i(x)$, $i = 1,2$ represent $mf$ as the crack tip enrichment functions. The first term technically applies to all nodes in the model, whereas the second term applies to nodes whose form function support crosses by the crack faces while the third and fourth terms are only applicable to nodes that cross at the crack tip.

The Heaviside function, $H(\xi)$ across the crack surfaces can be expressed as the following sign function:

$$H(\xi) = \begin{cases} 1, & if \quad \xi \geq 0 \\ -1, & otherwise \end{cases} \tag{9}$$

where $\xi = n(x - x^*)$, is the local axis perpendicular to the crack growth direction, $x$ is a Gauss point, $x^*$ is the point on the crack closest to $x$, and $n$ is the unit outward normal to the crack at $x$. Furthermore, the isotropic function of the asymptotic

crack, $F_\alpha(r,\theta)$, is:

$$F_\alpha(r,\theta)=\sqrt{r}\left[\sin\frac{\theta}{2},\cos\frac{\theta}{2},\sin\theta\sin\frac{\theta}{2},\sin\theta\cos\frac{\theta}{2}\right] \tag{10}$$

where $(r,\theta)$ is a polar coordinate system with its origin at the crack tip (as shown in Fig. 1).

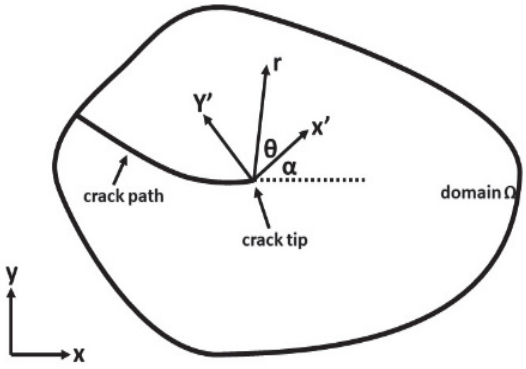


Figure 1: Polar coordinate at the crack tip [15].

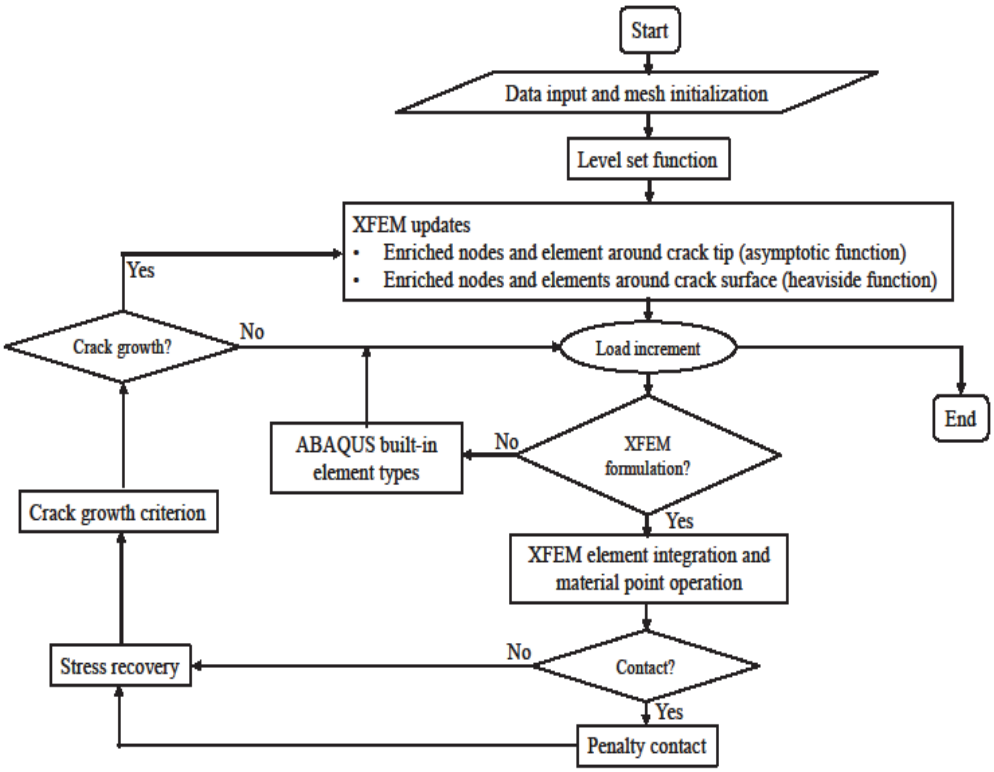


Figure 2: XFEM flowchart [16].

The XFEM formulation procedure is illustrated in Fig. 2. In the case of XFEM elements, there may be changes in position and number of Gauss points between load increments as the crack extends. Therefore, updating material state variables is done continuously until the load increments are completed. Whereas in crack propagation, the crack crosses the entire element that allows a reduced integration element to operate on plane problems such that stresses and strains are estimated in the middle of the element (on the integration point). Furthermore, for the crack tip located outside of the element, it is unnecessary to take into account the singularity of the stresses when defining the elemental displacements [9]. To keep from having to model the

stress singularity, the crack must propagate throughout an entire element. Therefore, the XFEM discontinuous displacement approximation in the crack propagation of plane problem is:

$$\boldsymbol{u} = \sum_{i=1}^{n} N_i(x) u_i + \sum_{j=1}^{m} N_j(x) H(\xi) a_j \tag{11}$$

where $N_i(x)$ is the nodal shape function, $N_j(x)$ is the new set of shape function associated with the enrichment part of the approximation. $u_i$ is the nodal displacement vector associated with the continuous part of the finite element solution, $H(\xi)$ represents a discontinuous jump function across the crack surfaces, $a_j$ is enriched nodal degree of freedom vector for modelling crack faces and two crack tips, respectively. $n$ is the number of nodes for each finite element, and $m$ is the set of nodes that have the crack face (but excludes the crack tip) in their support domain.

The onset and direction of the crack extension must be specified in simulating the degradation and eventual failure of an enriched element during the computational simulation of the XFEM formulation. The failure mechanism is made up of two ideas: a crack initiation criterion and a damage evolution law. Cracking develops when stresses or strains fulfill certain crack initiation criteria as specified by the traction-separation law damage. Subsequently, once the associated initiation criterion is met, the pace at which the cohesive stiffness degrades is described by the damage evolution law as specified by the displacement or energy release rate criterion.

## NUMERICAL SIMULATION OF CREEP FRACTURE INITIATION AND CREEP CRACK GROWTH

### *Rectangular plate with a single crack*

Fig. 3 shows a rectangular plate with a single crack with measurements, L=114.3 mm, W=25.4 mm and a=2 mm. Super alloy Inconel 800H at 650°C with E=154 GPa and v=0.33 was used as a specimen material. The creep model's power law is as shown in Eqn. 1, with the creep coefficient B=1.34 x $10^{-30}$ (stress in MPa) and n=5. Yang et al. [17] and Meng et al. [11] had previously investigated the similar model. The damage of the traction-separation laws for the crack initiation and evolution is selected on the basis of the maximum principal stress (MAXPS) criterion with yield strength, $\sigma_y$=93 MPa and a 0.3 mm failure displacement.

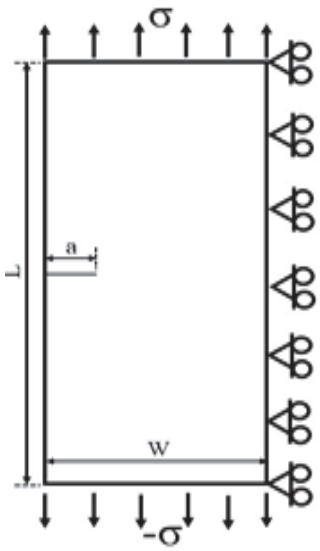


Figure 3: Geometry representation and boundary condition for rectangular plate specimen.

The elements are of linear quadrilateral four-node type with decreased integration, while fully integrating the elements and sub-elements (integrating richer elements). The C*-integral here was 8.37E-03 kJ/(m²h) with a stress intensity factor of =19.37 MPa.√m [23]. The values of the C(t)-integral gained from the domain form of the interaction integrals by employing the XFEM technique in the simulation and both short-time estimation and approximate interpolation formulas are presented in Fig. 4.

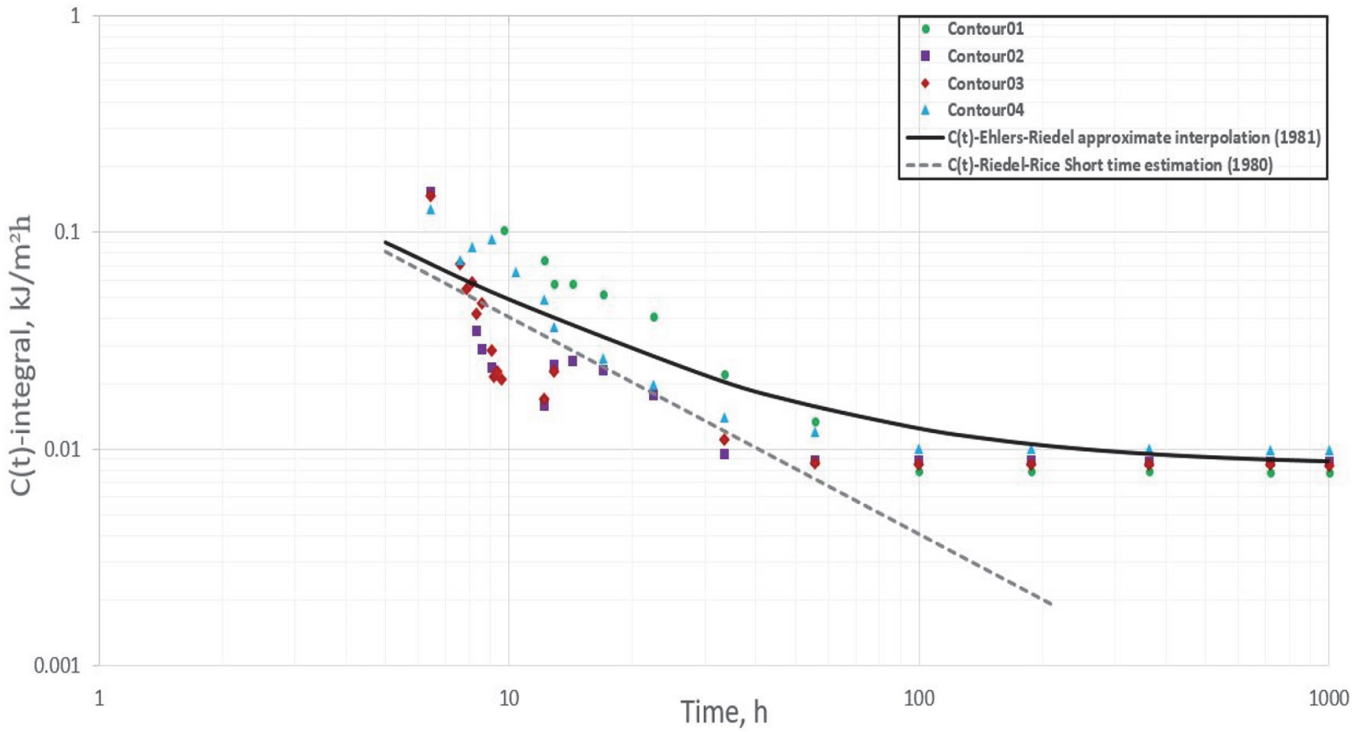


Figure 4: Solutions of the log-log plot of C(t)-integral near the crack tip in a rectangular plate with a single crack under plane stress.

As shown in Fig. 4, the results for the short times creep acquired from the three methods, which also includes the contours plotted, are strongly correlated. As for the long loading times, the results of the Ehler-approximation Riedel's interpolation and the steady-state value C* approach are moderately correlated with the XFEM solution. Furthermore, under the constant load, the values of C(t) indicated a declining trend as time increased. This suggests that while the load was maintained, the following creep deformation resulted in the crack tip stresses to relax. As shown in Fig. 5 and Fig. 6, the contour plots of the stress in the y-direction and the displacement magnitude are shown alongside the specimen's crack path. The crack spreads outwards from the center, with the most stress centered at the specimen's crack tip.

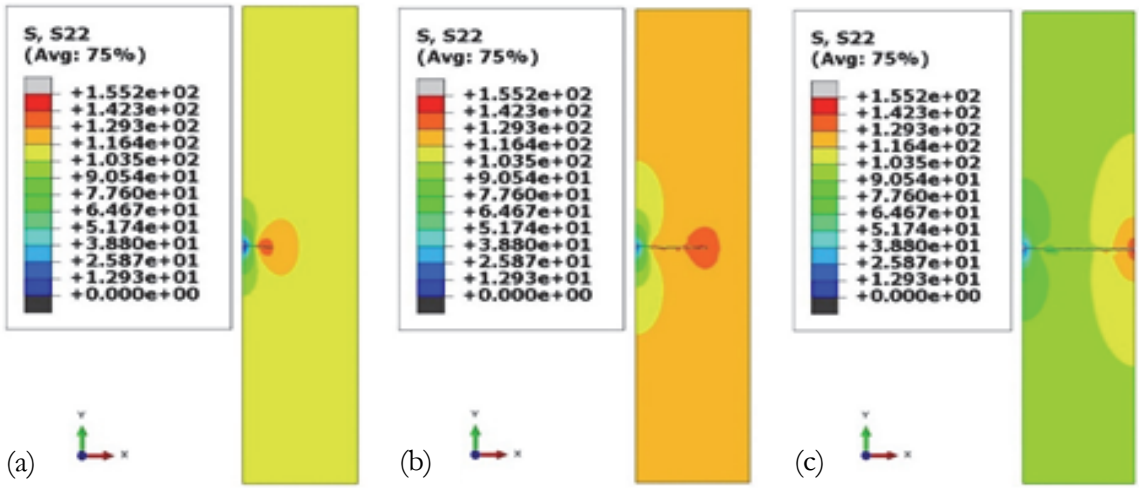


Figure 5: Rectangular plate with a single crack: contour of stress in y-direction along the crack at (a) t=114 h, (b) t=556 h and (c) t=998 h

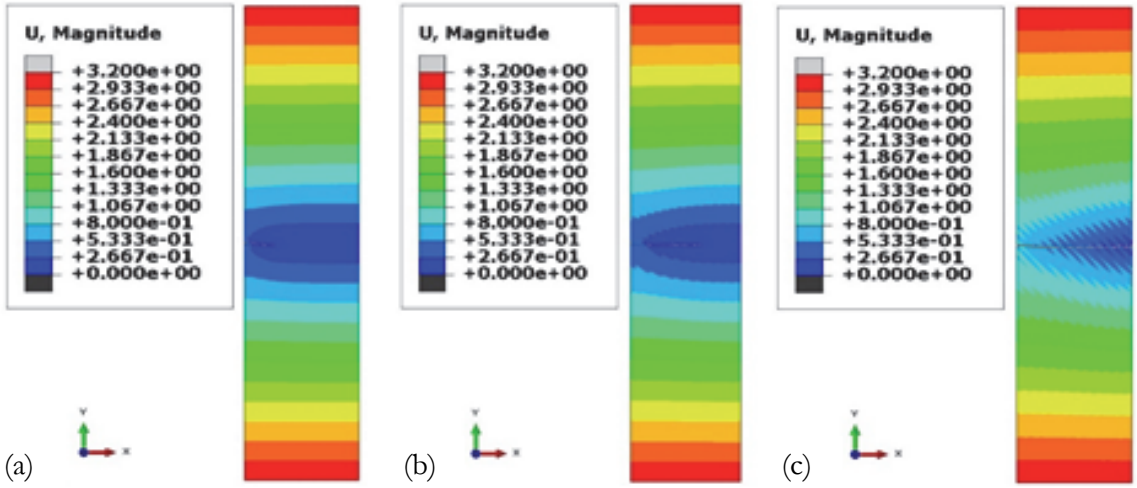


Figure 6: Rectangular plate with a single crack: contour of a magnitude of displacement along the crack at (a) t=114 h, (b) t=556 h and (c) t=998 h

*Compact tension (CT) specimen*

As shown in Fig. 7, a compact tension (CT) specimen of ASME P92 steel welded joint, with W=20 mm, L=24 mm, ϕ=5 mm and a=10 mm employed at 650°C to further proceed with the creep crack growth study. The load P=2050 N is administered to the CT-specimen with an analytical pin connected to the specimen's hole to represent the bolt in the experiment, while a plane stress is applied on the linear four-node quadrilateral elements.

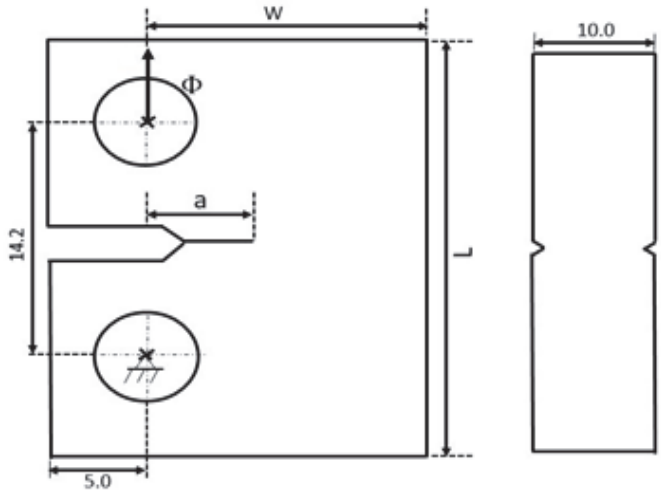


Figure 7: 2D-discretization domain of the specimen consisting of 5937 elements and 12380 nodes. A boundary condition in the upper hole was fixed at the x-axis (U1=0), while in the bottom hole it was fixed in all directions (U1, U2, RU2=0,0,0).

Zhao et al. [18] and Yatomi et al. [19] had thoroughly examined the creep crack growth in such specimen by means of an FEM analysis using node release technique. Whereby Zhao et al. [20] had investigated the experimental setup with $E$= 125 GPa, $\nu$=0.33, $B$=2.6353E-16 and $n$=5.23 being the material and creep properties. The damage for the traction-separation laws based on the maximum principal stress criterion (MAXPS) is applied to the enrichment elements with yield strength, $\sigma_y$ = 140 MPa and a failure displacement of 0.2 mm to introduce a crack initiation and evolution.

Starting with the explicit time integration, the program then automatically transitioned to the implicit thus permitted longer time increments and became stable. As can be seen in Fig. 8 and Fig. 9, the contour plots of the stress in the y-direction and the displacement magnitude become visible, spreading along the crack path. Once the stress value at the contour of the crack tip area reached its maximum stress concentration zone (SCZ) under the tensile load, the crack will start to expand and evenly spread at the infinity parallel to the crack direction.

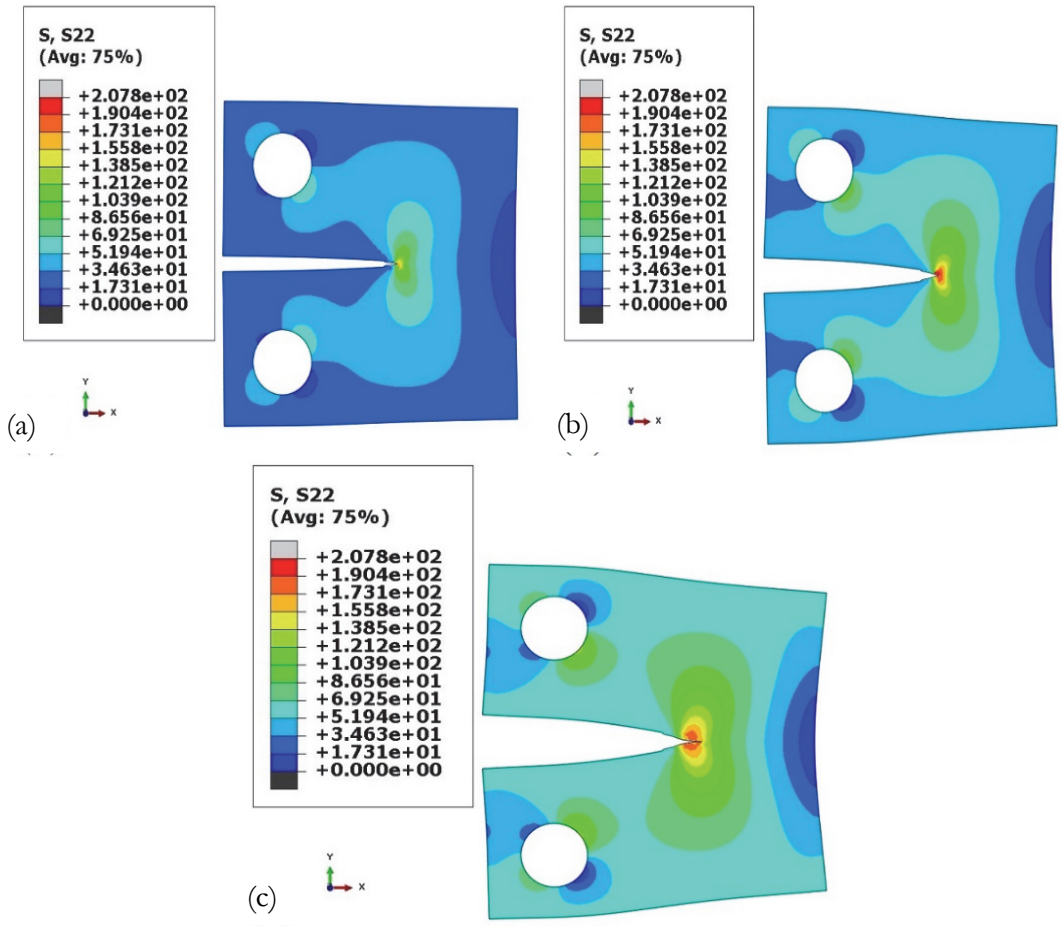


Figure 8: CT specimen: distribution of stress in y-direction along the crack at (a) t=24 h, (b) t=64 h and (c) t=100 h

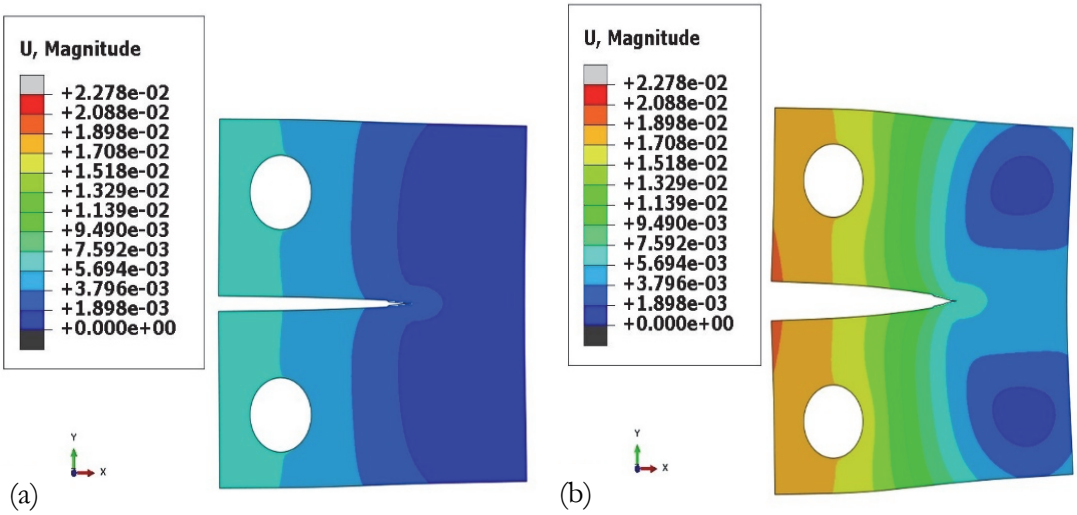

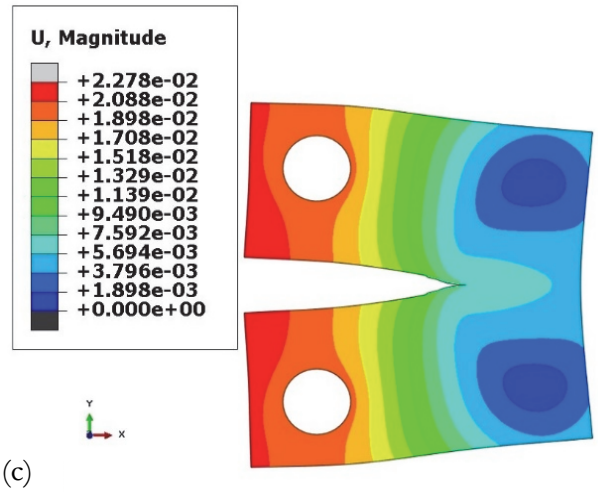


(c)

Figure 9: CT specimen: distribution of a magnitude of displacement along the crack at (a) t=24 h, (b) t=64 h and (c) t=100 h.

Furthermore, when the relation of creep crack growth length pertaining to normalized time is plotted (Fig. 10), the XFEM solutions and the experimental results are comparatively well estimated. The increase trend of the creep crack growth length with the rising normalized time can be seen in Fig. 10, represented by the current loading time, $t$ and the life, $t_f$ of each specimen's creep crack growth. Fig. 11 shows the representative creep crack growth rate with respect to C(t) for the XFEM solution and experimental results. The XFEM solution curve appears similar to that of the experimental results, bringing the R-squared value closer to 1. In essence, the pattern of the curves shows consistent creep crack propagation of the specimen.

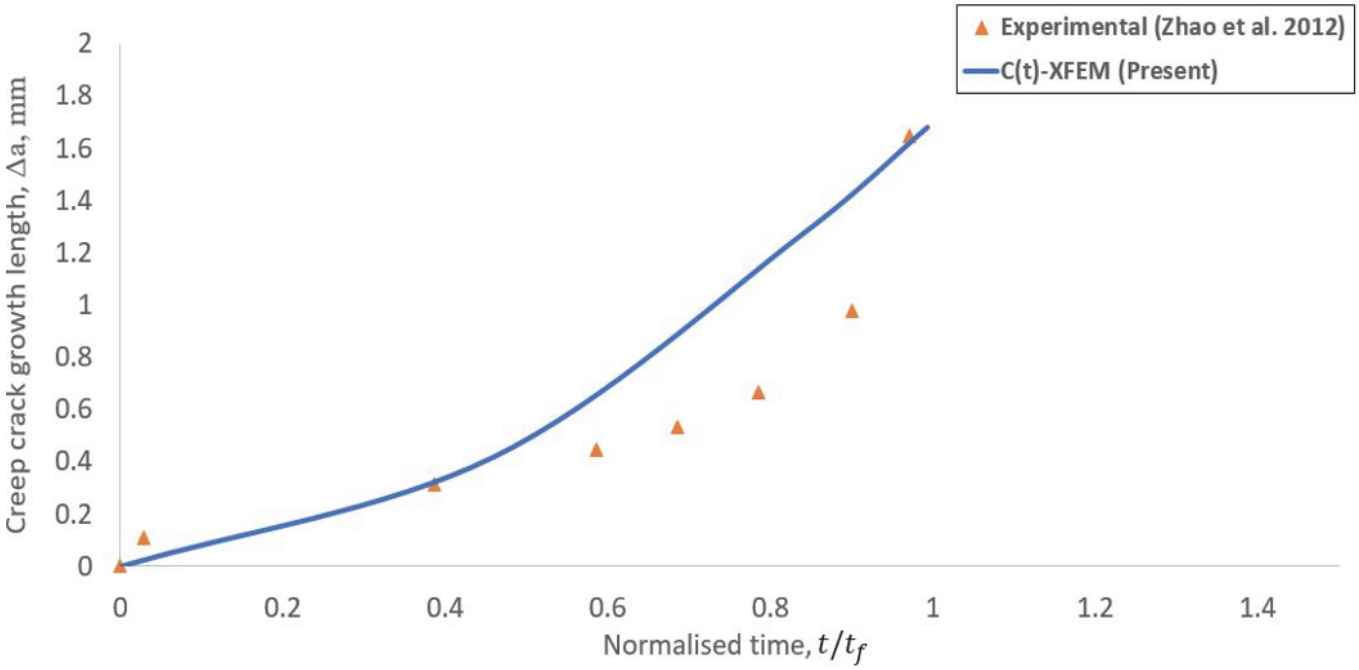


Figure 10: Relationship between XFEM calculated creep crack growth length and normalized time

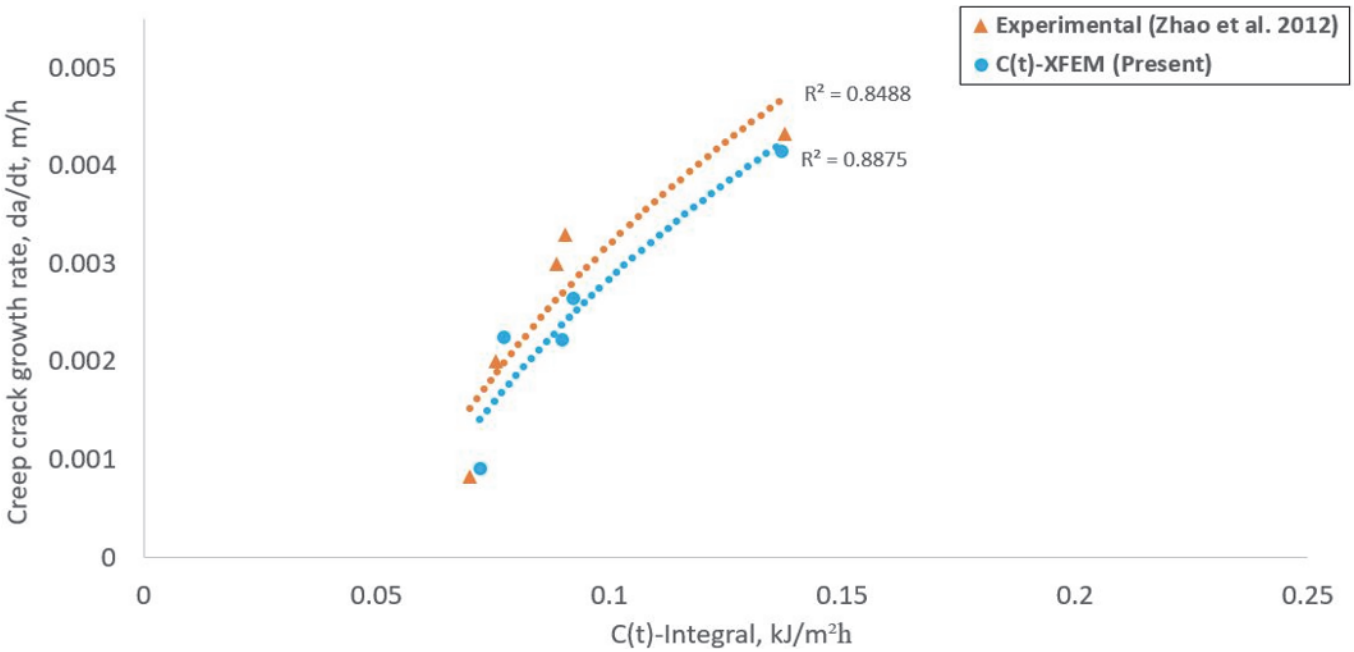


Figure 11: Comparison of XFEM calculated creep crack growth rate versus C(t)-integral with experimental data.

## Conclusion

The approach applied to investigate creep fracture initiation and predict creep crack growth of the ductile materials was numerical constitutive model. The creep fracture initiation was characterized by means of C(t)-integral and the materials' crack propagation that shows power-law creep behavior was predicted by formulating the XFEM solutions.

The analysis had identified a rectangular plate with single crack displaying a relationship between the XFEM solutions and analytical approximation based on short time estimation and Ehler-Riedel's approximate interpolation which relatively consistent with one another. The contour plot sequences of the stress in the y-direction and displacement magnitude were identified in addition to the crack path. At this point, there was an apparent crack evolution movement at the center of the specimen along with an increase in the distributed stress at the crack tip area.

In this study, a CT-specimen has been tested further, showing respectively the contour of the stress plots in the y-direction and the displacement magnitude. The trend of the propagation of the creep crack was well forecast and shown in the graph relations. In the first graph of the CT-specimen, the crack growth length with normalized time is shown where the XFEM solutions were properly estimated with the experimental data. Whereas the second graph shows the creep crack growth rate with C(t)-integral which produced a similar result when the two approaches were compared, bringing the R-squared value closer to 1. Thus, the C(t)-integral and XFEM formulation relationship had facilitated in predicting the ductile materials' creep crack initiation and creep crack growth behaviour and subsequently verified the results of the study. The next analysis regarding creep material behaviour will be conducted by representing the damage parameters of creep failure in the ductile materials with the constitutive creep damage model based on continuum damage model.

## Acknowlegement

This work is supported by Universiti Kebangsaan Malaysia under Geran Galakan Penyelidik Muda (GGPM), GGPM-2019-059.

## REFERENCES


[1] Yao, H.T., Xuan, F.Z, Wang, Z and Tu, J.S. (2007). A Review of Creep Analysis and Design under Multi-Axial Stress States, Nuclear Engineering and Design, 237(18), pp. 1969-1986.

[2] Hsu, T.R and Zhai Z.H. (1984).A Finite Element Algorithm for Creep Crack Growth, Engineering Fracture Mechanics, 20(3), pp. 521-533.

[3] Hollstein, T. and Kienzler, R. (1988). Fracture Mechanics Characterisation of Crack Growth under Creep Conditions, The Journal of Strain Analysis for Engineering Design, 23(2), pp. 87-96.

[4] Yatomi, M., Davies, C.M., and Nikbin, K.M. (2008). Creep Crack Growth Simulations in 316H Stainless Steel, Engineering Fracture Mechanics, 75(18), pp. 5140-5150.

[5] Zhang, J.W., Wang, G.Z., Xuan, F.Z., and Tu, S.T. (2014). Prediction of Creep Crack Growth behaviour in Cr-Mo-V steel speci-mens with different constraints for a wide range of C, Engineering Fracture Mechanics, 132, pp. 70-84.

[6] Curiel-Sosa, J.L. and Karapurath, N. (2012). Delamination Modelling of GLARE using The Extended Finite Element Method, Composites Science and Technology, 72(7), pp. 788-791.

[7] Giner, E., Sukumar, N., Tarancon, J., and Fuenmayor, F. (2009). An Abaqus Implementation of the Extended Finite Element Method, Engineering Fracture Mechanics, 76(3), pp. 347-368.

[8] Farukh, F., Zhao, L.,Jiang, R., Reed, P., Proprentner, D. and Shollock, B. (2015). Fatigue Crack Growth in a Nickel-based Superalloy at Elavated Temperature-Experimental Studies, Viscoplasticity Modelling and XFEM Predictions, Mechanics of Advanced Materials and Modern Processes, 1(2), pp. 2.

[9] Moreno, M.C.S., Curiel-Sosa, J.L., Navarro-Zafra, J., Vicente, J.L.M. and Cela, J.J.L. (2015). Crack Propagation in a Chopped Glass-Reinforced Composite under Biaxial Testing by Means of XFEM, Composite Structure, 119, pp. 264-271.

[10] Pandey, V., Singh, I., Mishra, B., Ahmad, S., Rao, A. and Kumar, V. (2017). Creep Crack Simulations using Continuum Damage Mechanics and Extended Finite Element Method, International Journal of Damage Mechanics, 0(0), pp. 1-32.

[11] Meng, Q. and Wang, Z. (2014). Extended Finite Element Method for Power-Law Creep Crack Growth, Engineering Fracture Mechanics, 127, pp. 148-160.

[12] Riedel, H. and Rice, J.R. (1980). Tensile Cracks in Creeping Solids, Fracture Mechanics: Twelfth Conference, ASTM STP 700, pp. 112-130.

[13] Ehlers, R. and Riedel, H. (1981). A Finite Element Analysis of Creep Deformation in a Specimen Containing a Macroscopic Crack, Advances in Fracture Research, Proceedings of the Fifth International Conference on Fracture, 2, pp. 691-698.

[14] Sukumar, N. and Prevost, J.H. (2003). Modeling Quasi-Static Crack Growth with The Extended Finite Element Method Part I: Computer Implementation, International Journal of Solids and Structures, 40(26), pp. 7513-7537.

[15] Ahmad, M.I.M., Curiel-Sosa, J.L., Arun, S. and Rongong, J.A. (2019). An Enhanced Void-Crack-Based Rousselier Damage Model for Ductile Fracture with the XFEM, International Journal of Damage Mechanics, 28(6), pp. 943-969.

[16] User's Guide Documentation, Dassault Systemes Simulia Corp. Abaqus, 6, 14-2, 2014.

[17] Yang, L., Sutton, M.A., Deng, X. and Lyons, J.S. (1996). Finite Element Analysis of Creep Fracture Initiation in a Model Superalloy Material, International Journal of Fracture, 81(4), pp. 299-320.

[18] Zhao, L., Jing, H., Han, Y., Xiu, J. and Xu, L. (2012). Prediction of Creep Crack Growth Behaviour in ASME P92 Steel Welded Joint, Computational Materials Science, 61, pp. 185-193.

[19] Yatomi, M., Yoshida, K. and Kimura, T. (2011). Difference of Creep Crack Growth Behaviour for Base, Heat-Affected Zone and Welds of Modified 9Cr-1Mo Steel, Materials at High Temperature, 28(2), pp.109-113.

[20] Zhao, L., Jing, H., Xiu, J., Han, Y. and Xu, L. (2014). Experimental Investigation of Specimen Size Effect on Creep Crack Growth behaviour in P92 Steel Welded Joint, Materials and Design, 57, pp. 736-743.